

Size limit of superparamagnetic inclusions in dust grains and difficulty of magnetic grain alignment in protoplanetary disks

HAIFENG YANG^{1,*}

¹*Institute for Advanced Study, Tsinghua University, Beijing, 100084, China*

(Received; Revised; Accepted)

ABSTRACT

Alignment of non-spherical grains with magnetic fields is an important problem as it lays the foundation of probing magnetic fields with polarized dust thermal emissions. In this paper, we investigate the feasibility of magnetic alignment in protoplanetary disks (PPDs). We use an alignment condition that Larmor precession should be fast compared with the damping timescale. We first show that the Larmor precession timescale is some three orders of magnitude longer than the damping time for millimeter-sized grains under conditions typical of PPDs, making the magnetic alignment unlikely. The precession time can be shortened by superparamagnetic inclusions (SPIs), but the reduction factor strongly depends on the size of the SPI clusters, which we find is limited by the so-called “Néel’s relaxation process.” In particular, the size limit of SPIs is set by the so-called “anisotropic energy constant” of the SPI material, which describes the energy barrier needed to change the direction of the magnetic moment of an SPI. For the most common iron-bearing materials, we find maximum SPI sizes corresponding to a reduction factor of the Larmor precession timescale of order 10^3 . We also find that reaching this maximum reduction factor requires fine-tuning on the SPI sizes. Lastly, we illustrate the effects of the SPI size limits on magnetic alignment of dust grains with a simple disk model, and we conclude that it is unlikely for relatively large grains of order $100\ \mu\text{m}$ or more to be aligned with magnetic fields even with SPIs.

Keywords: Protoplanetary disks — ISM: magnetic fields — Polarization

1. INTRODUCTION

The polarization of starlight was first observed in 1949 (Hiltner 1949). It was soon attributed to the alignment of dust grains in the foreground interstellar medium. Since then, the alignment of dust grains, especially with respect to magnetic fields, has many developments. Many theories were developed to explain how dust grains are aligned with magnetic fields, such as Davis-Greenstein mechanism (Davis & Greenstein 1951), hydrogen formation torque (Purcell 1979), radiative alignment torque (B-RAT; Dolginov & Mytrophanov 1976; Draine & Weingartner 1997; Lazarian & Hoang 2007), and recently mechanical alignment torque (B-MAT; Hoang et al. 2018). We refer interested readers to Andersson et al. (2015) and references therein.

Superparamagnetism (SPM) was first introduced to the astronomical literatures of grain alignment by Jones & Spitzer (1967). They pointed out that SPM can enhance magnetic relaxation, the process invoked by Davis-Greenstein mechanism to dissipate oscillating magnetic moments and to align grains, which was found insufficient to align regular paramagnetic dust grains with magnetic fields. Mathis (1986) adopted this theory with the assumption that grains containing any small superparamagnetic particle, the so-called superparamagnetic inclusions (SPIs), can be aligned with magnetic fields. Under this theory, the fact that bigger grains are better aligned is well explained since bigger grains are more likely to contain SPIs. Fe-Ni inclusions appear to present in interplanetary dust particles, and their spatial frequency supports Mathis’s theory in explaining the wavelength dependence of polarization (Goodman & Whittet 1995). Magnetic nanoparticles and inclusions were also discussed recently by Draine & Hensley

Corresponding author: Haifeng Yang
yanghaifeng@tsinghua.edu.cn

* C.N. Yang Junior Fellow

(2013) focusing on the impacts of such inclusions on the dust thermal emission and polarization.

Observationally, tracing magnetic fields with polarized thermal emission from grains aligned with magnetic fields is a classical and successful method. It is clear that grains in diffuse interstellar medium are aligned with magnetic field from starlight polarization (Mathewson & Ford 1970). Recently, this picture receives firm supports from the Planck all-sky survey data (Planck Collaboration et al. 2015), and from the interferometric polarimetry data (see Hull & Zhang 2019 and reference therein). It is in no doubt that grains on scales larger than disks are aligned with magnetic fields.

In the past six years, thanks to the improvement of interferometric polarimetry, especially with the Atacama Large Millimeter/submillimeter Array (ALMA), we have become able to resolve polarization maps down to the disk scale. The results have been surprising. Most systems show uniform polarization patterns, especially at shorter wavelengths, e.g. HL Tau (Stephens et al. 2014; Stephens et al. 2017), IM Lup (Hull et al. 2018), DG Tau (Bacciotti et al. 2018), and HD163296 (Dent et al. 2019), which are better explained with the self-scattering of dust grains than with magnetically aligned grains (Kataoka et al. 2015; Yang et al. 2016a; Ohashi & Kataoka 2019; Lin et al. 2019). Cox et al. (2018)’s survey found a trend that the polarization is uniform on scales smaller than 100 AU at percent level, whereas the polarization is less organized on larger scales at a higher level ($\sim 5\%$). This is consistent with the picture that dust grains at disk scales are not aligned. There are also some systems showing complicated polarization features, such as the binary system BHB07-11 (Alves et al. 2018), the southern part of HD142527 (Kataoka et al. 2016; Ohashi et al. 2018), and HL Tau (Kataoka et al. 2017). However, the origin of these additional complexities is not certain at this time.

Theoretically, the transition from magnetic alignment to no-magnetic-alignment going from the more diffuse surrounding region to the disk is not surprising. The protoplanetary disk (PPD) environment is very different from the diffuse ISM in many ways: higher density, bigger grain sizes, different temperature and radiation energy density, etc. A rough comparison given in Sec. 2 shows that the Larmor precession timescale can be some three orders of magnitude larger than the gaseous damping timescale, making magnetic alignment impossible (see also Tazaki et al. 2017). Hoang (2017) pointed out that if the dust grains contain large SPIs (on the order of 10^5 iron atoms each), magnetic alignment of millimeter dust grains can still be possible in PPDs. The enhancement from SPIs strongly depends on the

size of each SPI. In this paper we will focus on estimating the maximum size of SPIs and discuss how the size limit affects the magnetic alignment of dust grains in PPDs.

The structure of this paper is as follows. In Sec. 2, we introduce the basic timescales involved in the magnetic alignment process, and give a simple comparison for regular paramagnetic materials. In Sec. 3, we introduce how SPIs can enhance the magnetic susceptibility and how the cluster size is limited by the relaxation process. In Sec. 4, we estimate the size limit of SPIs assuming a few commonly adopted forms of iron. In Sec. 5, we adopt a simple disk model and discuss the feasibility of magnetic alignment in PPDs. In Sec. 6, we discuss caveats and uncertainties in this work, as well as its implications for several observed disks. We summarize our results in Sec. 7.

2. BASIC MAGNETIC ALIGNMENT THEORY

2.1. Criteria for magnetic alignment

Dust grain alignment with magnetic fields is a complicated process with many timescales involved. An outline of the process (regardless of alignment mechanism) is as follows (see e.g. Lazarian 2007). Initially, a randomly-spinning dust grain nutates about its angular momentum axis. Over a timescale t_{int} , the principal axis of the dust grain becomes aligned with its angular momentum through some relaxation processes. The dust grain’s angular momentum also precesses around the external magnetic field on the Larmor precession timescale (t_L). At the end, some torques gradually force the angular momentum of the dust grain to be aligned with the magnetic field, over a timescale of t_{al} . At the same time, the random bombardment of gas particles tries to disturb the angular momentum, over the gaseous damping timescale (t_d).

One typically considers that these three timescales must follow a hierarchical inequality – i.e., $t_L < t_{\text{al}} < t_d$ – in order for grain alignment to proceed successfully. However, the alignment timescale t_{al} is considerably more complicated than the other two timescales to compute in general, because it depends on the specific torquing mechanism at play. For the purpose of this paper, we work with the insufficient but still necessary condition $t_L < t_d$ to determine conditions under which dust grains can align with ambient magnetic fields¹. Even though $t_L > t_d$ is unrealistic in most interstellar medium, it becomes a strong possibility in PPDs

¹ Note that this criterion effectively ignored the suprathermal rotation, which will be discussed in Sec. 6.

as grains grow to millimeter in size and gas density increases by many orders of magnitude compared with the ISM values, as we will see more quantitatively in the following section.

In theoretical works studying the dynamics of magnetic grain alignment, fast Larmor precession has been mostly assumed, so that the calculated torques are averaged over one precession before the dynamics of the dust grain is studied (e.g., [Lazarian & Hoang 2007](#); [Hoang et al. 2018](#)). In this work, we use $t_L < 0.1t_d$ as the criterion for fast Larmor precession assumption. In this regime, the Larmor precession timescale will not be the limiting factor, and magnetic grain alignment becomes possible. We will come back to discuss this criterion and its caveats in more detail in Sec. 6.

2.2. Gaseous damping timescale

The random bombardment of gas particles on dust grains tends to misalign any ordered orientation of the dust grains. This happens roughly on a timescale of ([Roberge et al. 1993](#)):

$$t_d = \frac{2\sqrt{\pi}}{5} \frac{\rho_s a}{n_g m_g v_{g,th}} = 3.54 \times 10^{12} \text{ s} \times \left(\frac{\rho_s}{3 \text{ g/cm}^3} \right) \times \left(\frac{a}{0.1 \text{ } \mu\text{m}} \right) \left(\frac{n_g}{20 \text{ cm}^{-3}} \right)^{-1} \left(\frac{T_g}{85 \text{ K}} \right)^{-1/2}, \quad (1)$$

where ρ_s is the mass density of the (solid) dust grain, a is the grain size, n_g is the number density of gas particles, and T_g is the gas temperature. This is a rather long time scale for the diffuse ISM conditions we used above. If we take a PPD with total mass of $0.01 M_\odot$ as normalization, uniformly distributed in a cylinder with 100 AU as radius and 10 AU as scale height, we have:

$$t_d = 2.6 \times 10^8 \text{ s} \times \left(\frac{\rho_s}{3 \text{ g/cm}^3} \right) \left(\frac{a}{1 \text{ mm}} \right) \times \left(\frac{n_g}{5 \times 10^9 \text{ cm}^{-3}} \right)^{-1} \left(\frac{T_g}{25 \text{ K}} \right)^{-1/2}, \quad (2)$$

which is shorter than typical dynamical timescales in PPDs.

2.3. Larmor precession timescale

The Larmor precession process is the precession of a magnetic moment around a magnetic field. A spinning dust grain possess a magnetic moment due to the Barnett effect ([Barnett 1915](#)). Its magnetization is $M = \chi\Omega/\gamma$ ([Draine 2004](#)), where χ is the magnetic susceptibility, Ω is the angular velocity, $\gamma = g\mu_B/\hbar$ is the

gyromagnetic ratio, and μ_B is the Bohr magneton. The g -factor is about 2 for electrons.

For regular paramagnetic material, the magnetic susceptibility follows Curie's Law ([Morrish 2001](#)):

$$\chi = \frac{n\mu^2}{3kT} = 10^{-3} \hat{\chi} \left(\frac{T}{25 \text{ K}} \right)^{-1}, \quad (3)$$

where n is the number density of magnetic units, μ is the magnetic moment of each unit, and $\hat{\chi}$ is a dimensionless parameter that is on the order of unity for regular paramagnetic materials ([Draine 1996](#); [Lazarian 2007](#)).

The Larmor precession timescale is then:

$$t_L = \frac{2\pi I \gamma}{\chi V B} = 4.3 \times 10^6 \text{ s} \times \hat{\chi}^{-1} \left(\frac{\rho_s}{3 \text{ g/cm}^3} \right) \times \left(\frac{T_d}{25 \text{ K}} \right) \left(\frac{B}{5 \text{ } \mu\text{G}} \right)^{-1} \left(\frac{a}{0.1 \text{ } \mu\text{m}} \right)^2. \quad (4)$$

We can see that this timescale is some six orders smaller than the gaseous damping timescale for parameters appropriate for the diffuse ISM. But if we normalize the field strength to 5 mG, which is typical for a PPD with $10^{-8} M_\odot/\text{yr}$ accretion rate at tens of AU scale ([Bai 2011](#)), and the grain size to 1 mm, we get:

$$t_L = 4.3 \times 10^{11} \text{ s} \times \hat{\chi}^{-1} \left(\frac{\rho_s}{3 \text{ g/cm}^3} \right) \times \left(\frac{T_d}{25 \text{ K}} \right) \left(\frac{B}{5 \text{ mG}} \right)^{-1} \left(\frac{a}{1 \text{ mm}} \right)^2, \quad (5)$$

which is about $10^3 t_d$.

3. SUPERPARAMAGNETIC INCLUSIONS

3.1. Basic picture

Superparamagnetic inclusions (SPIs) are small (nano-sized) particles of ferromagnetic material². Within one such particle, all the atoms are spontaneously magnetized and behave like a single large magnetic moment, the so-called ‘‘macro-spin’’ ([Bean & Livingston 1959](#)). They are not big enough to create domain walls yet, and are usually referred to as ‘‘single-domain particles’’. In the absence of external magnetic fields, these macro-spins are randomly oriented and behave like paramagnetic materials as an ensemble.

Let's first consider the simplest case, where an SPI has no preferred direction for magnetization. This isotropic

² In this work, we don't distinguish ferromagnetic material with ferrimagnetic material, or even speromagnetic material. They all behave as macro-spins, as discussed in the text, but maybe with different number of effective Bohr magneton per atom (p in Eq.(7)).

case is mathematically identical to the regular paramagnetic case, and we have the bulk magnetic susceptibility of an ensemble of identical SPIs as (Jones & Spitzer 1967):

$$\chi_{sp} = \frac{N\mu^2}{3kT}, \quad (6)$$

where N is the number density of SPIs inside the dust grain. Let n_{tot} be the total number density of atoms and assume a fraction of f_{sp} atoms are magnetic atoms embedded in SPIs. Let μ be the magnetic moment of the “macro-spins”. If each SPI contains N_{cl} magnetic atoms, we have $N = f_{sp}n_{tot}/N_{cl}$, and $\mu = N_{cl}p\mu_B$, where $p\mu_B$ is the averaged Bohr magneton for each magnetic atom. With these we have (Draine 1996):

$$\begin{aligned} \chi_{sp} &= \frac{f_{sp}n_{tot}N_{cl}(p\mu_B)^2}{3kT} \\ &= 0.72 \times 10^{-2} N_{cl} f_{sp} \left(\frac{n_{tot}}{10^{23} \text{ cm}^{-3}} \right) \left(\frac{p}{3} \right)^2 \left(\frac{T}{25 \text{ K}} \right)^{-1}. \end{aligned} \quad (7)$$

Compared with Eq. (3), we have:

$$\hat{\chi} = 7.2 N_{cl} f_{sp} (p/3)^2. \quad (8)$$

In reality, SPIs will have a preferred direction for magnetization. For example, a prolate particle prefers to be magnetized along its long axis (Bean & Livingston 1959). This is called shape anisotropy. Another example is metallic iron, which has a cubic crystalline structure. Metallic iron has less energy when magnetized along one of the principal axes of its crystalline structure (so-called “easy axis”, Dai & Qian 2017). This is called magnetocrystalline anisotropy.

Even though the energy would be different in the presence of anisotropy, the susceptibility remains the same in thermal equilibrium states. Let K be the so-called “anisotropy constant”, such that KV is the energy needed to change the direction of the magnetic moment. With a simple prescription, Bean & Livingston (1959) showed that the ensemble-averaged magnetic susceptibility remains the same for both of the two limiting cases, when $KV \gg kT$ and when $KV \ll kT$. Thus Eq. (7) works even for anisotropic SPIs.

3.2. Size limit determined by the relaxation process

Billas et al. (1994) showed that single-domain particles as small as $N_{cl} = 30$ can show superparamagnetism. In this subsection, we will discuss what determines the maximum size for SPI, which is more important than lower limit.

Néel (1949) first proposed that single-domain particles experience random Brownian-like motions that can

change the orientation of its magnetic moment (see also Bean & Livingston 1959). This happens on a timescale (the so-called “Néel’s relaxation timescale”) of:

$$t_N \equiv t_0 \exp \left(\frac{KV}{kT} \right), \quad (9)$$

where t_0 is called “attempt timescale” typically on the order of 10^{-9} s. Setting the t_N equal to the timescale of interest (τ), we can define a critical blocking volume as:

$$V_{cr} = \frac{kT}{K} \ln \left(\frac{\tau}{t_0} \right). \quad (10)$$

The typical dynamical timescale of a 100 AU sized PPD is about 1000 yr, which yields $\ln(\tau/t_0) \approx 45$. We can see that the critical volume strongly depends on the temperature, and the cluster size measured at room temperature doesn’t apply directly to an astronomical environment, which hasn’t been considered before. The critical number of magnetic atoms can then be calculated, for iron-based ferromagnetic material, through:

$$N_{cr} = \frac{\rho V_{cr} f_{Fe}}{56m_p} = \frac{\rho f_{Fe} kT}{56m_p K} \ln \left(\frac{\tau}{t_0} \right), \quad (11)$$

where f_{Fe} is the mass fraction of iron atoms in the ferromagnetic material constituting the SPIs, and $56m_p$ is the mass of an iron atom.

The magnetization of a dust grain with SPIs is illustrated with a simplified model in Fig. 1. In this model, we consider two dust grains with uniformly sized SPIs. The left one has smaller SPIs, whereas the right one contains bigger SPIs. At $t < 0$, there is no external magnetic field. The magnetic moment of each SPIs are randomly oriented such that both dust grains have no bulk magnetization. At $t = 0$, we turn on external magnetic fields, and observe the magnetization of dust grains at τ , the dynamical timescale of our interest. We will find that all the small SPIs in the left dust grain turn into the external magnetic field direction (with thermal fluctuation). The resulting magnetic susceptibility of the dust grain is the superparamagnetic susceptibility $\chi_{sp}(N_{cl})$ in Eq. (7). In contrast, the large SPIs in the right dust grain do not have enough time to overcome the anisotropic energy barrier. Their magnetic moments are effectively “blocked” and do not contribute to the magnetization of the dust grain. The dependence of the magnetic susceptibility on the size of SPI clusters can be approximated as (see Appendix A for a more quantitative discussion):

$$\chi = \begin{cases} 0, & N_{cl} > N_{cr} \\ \chi_{sp}(N_{cl}), & N_{cl} < N_{cr} \end{cases}. \quad (12)$$

We can see that the maximum enhancement of the magnetic susceptibility for an ensemble of SPIs of equal sizes is:

$$\chi_{\max} = \chi_{sp}(N_{cr}), \quad (13)$$

which is achieved when all SPIs in a dust grain are of the same size with N_{cr} magnetic atoms.

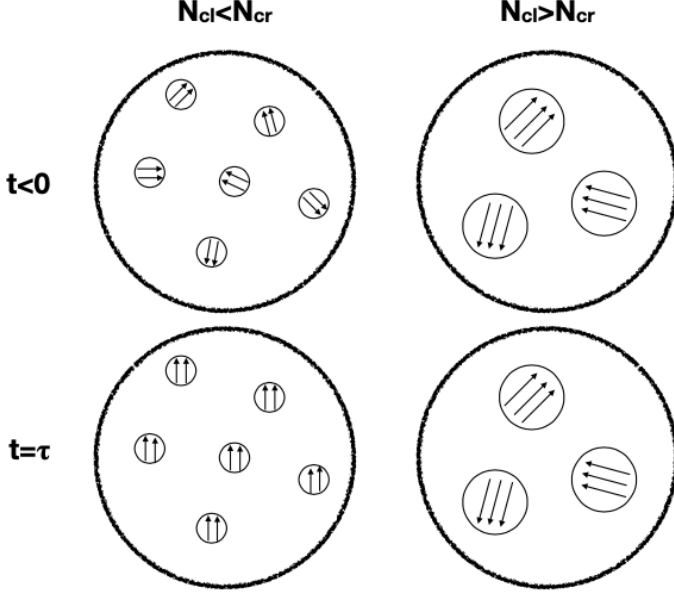


Figure 1. A schematic illustration of the magnetization of dust grains with SPIs of different sizes. The left column represents a dust grain with small SPIs. The right column represents a dust grain with big SPIs. The top row is their initial states before applying external magnetic fields. Starting from $t = 0$, an external magnetic field going up is applied. The bottom row is the magnetization of these two dust grains at time τ , the dynamical timescale of interest.

3.3. Distribution of SPIs

So far we have only considered ensembles of SPIs with the same size. In order to understand the effects of a distribution of SPI sizes, we adopt a very simple power-law distribution with index $-q$: $dn(N_{cl})/dN_{cl} = CN_{cl}^{-q}$, with $N_1 < N_{cl} < N_2$ is the cluster size and C is an arbitrary constant to be determined from the iron abundance.

We are particularly interested in the scenario when $N_1 < N_{cr} < N_2$. With Eq. (12), the magnetic susceptibility of this ensemble of SPIs can be calculated as:

$$\begin{aligned} \chi &= \frac{1}{B} \int_{N_1}^{N_2} \frac{dn(N_{cl})}{dN_{cl}} \langle \mu_z \rangle dN_{cl} \\ &= \int_{N_1}^{N_{cr}} C N_{cl}^{-q} \frac{N_{cl}^2 p^2 \mu_B^2}{3kT} dN_{cl} \\ &= \frac{C p^2 \mu_B^2}{3(3-q)kT} N_{cl}^{3-q} \Big|_{N_1}^{N_{cr}}, \end{aligned} \quad (14)$$

where $\langle \mu_z \rangle$ is the averaged magnetic moment along magnetic field direction (see Appendix for more detail). With some arithmetic of finding the constant C , we can express our results as:

$$\chi = \chi_{\max} \times \begin{cases} \frac{2-q}{3-q} \left(\frac{N_{cr}}{N_2} \right)^{2-q}, & q < 2; \\ \frac{q-2}{3-q} \left(\frac{N_1}{N_{cr}} \right)^{q-2}, & 2 < q < 3. \end{cases} \quad (15)$$

We can see that the end magnetic susceptibility of this ensemble is always smaller than χ_{\max} . The reduction factor is roughly the ratio of the number density of iron atoms within SPIs with sizes close to N_{cr} to the total number density of iron atoms within SPIs. Because of this reduction factor, reaching the maximum value of $\chi_{sp} = \chi_{\max}$ implicitly assumes that all SPIs have sizes close to the critical size N_{cr} .

4. ESTIMATE THE CRITICAL SIZE OF SPIS

The critical size of an SPI is an important quantity for determining how big of an enhancement it will have on the magnetic susceptibility of the host dust grain. In this section we perform estimates of SPI critical sizes, in terms of the number of magnetic atoms N_{cr} , for various materials that might plausibly be contained in astrophysical dust grains.

As seen in Eq. (10), the anisotropy constant K determines the critical volume, when the temperature is fixed. In nature, there are two most important contributions to K : the shape anisotropy and the magnetocrystalline anisotropy. In this work, we will ignore the first one and assume spherical SPIs. Including the shape anisotropy will increase the anisotropy constant and decrease the size estimates given below. In other words, our estimates are conservative upper limits.

The critical volume is defined in Eq. (10) and values at 25 K are reported here. We assume room temperature densities of stoichiometric materials. Besides the critical number of magnetic atoms in one SPI (N_{cr}), we also report the magnetic susceptibility χ_{\max} , taking $f_{sp} = 0.1$, and $n_{tot} = 10^{23} \text{ cm}^{-3}$.

4.1. Fe_3O_4 (magnetite)

At low temperature ($T < 120$ K), magnetite has a monoclinic structure (Iizumi et al. 1982). The magnetic anisotropy energy was determined by Abe et al. (1976) as:

$$E_a = K_a \alpha_a^2 + K_b \alpha_b^2 + K_{aa} \alpha_a^4 + K_{bb} \alpha_b^4 + K_{ab} \alpha_a^2 \alpha_b^2 - K_u \alpha_{111}^2, \quad (16)$$

with $K_a = 25.2$, $K_b = 3.7$, $K_u = 2.1$, $K_{aa} = 1.8$, $K_{bb} = 2.4$, and $K_{ab} = 7.0$ in 10^5 erg/cm³, and all α 's are directional cosines (see Abe et al. 1976 for their definitions). The easy axes are along (001) and (00 $\bar{1}$) directions. The magnetization can change from one easy axis to another through saddle points along (010) or (0 $\bar{1}$ 0) directions, and the energy barrier is $K \approx 6.1 \times 10^5$ erg/cm³. This translates to a critical volume as $V_{\text{cr}} = 2.5 \times 10^{-19}$ cm³. Li et al. (2007) found a spin density as $3.54 \mu_B$ per formula at 10 K along [100] direction, which we will use in this paper. For every iron atom, we have $p = 1.18$ Bohr magnetons. Taking $\rho = 5.17$ g/cm³, we get $N_{\text{cr}} = 1.0 \times 10^4$ and $\hat{\chi}_{\text{max}} = 1.1 \times 10^3$.

4.2. γ -Fe₂O₃ (maghemite)

γ -Fe₂O₃ (maghemite) is ferrimagnetic iron oxide with similar structures to magnetite at room temperature. Its formula is often supposed to be $(\text{Fe}^{3+})_{\text{A}}(\text{Fe}_{5/3}^{3+} \square_{1/3})_{\text{B}}\text{O}_4$, where \square represents a vacancy. A perfect crystal has $3.33 \mu_B$ per formula. Hence we have $p = 1.25$. In bulk samples, the moments were usually found to be about 87 ~ 94% of this value (Coe & Khalafalla 1972). Pisane et al. (2017) fitted the effective magnetic anisotropy as a function of particle size with three terms. The leading term (and the dominating term for big particles) corresponds to $K = 1.9 \times 10^5$ erg/cm³. This translates into a critical volume of $V_{\text{cr}} = 8.2 \times 10^{-19}$ cm³. Taking $\rho = 4.9$ g/cm³, we have $N_{\text{cr}} = 3.0 \times 10^4$, and $\hat{\chi}_{\text{max}} = 3.7 \times 10^3$.

4.3. Metallic iron

The leading term in the magnetic anisotropy energy of metallic iron has the form of $K_1(\alpha_1^2 \alpha_2^2 + \alpha_2^2 \alpha_3^2 + \alpha_1^2 \alpha_3^2)$, where α_i , $i = 1, 2, 3$ are directional cosines. At temperatures below 100 K, $K_1 \approx 5.4 \times 10^5$ erg/cm³ (Dai & Qian 2017). The energy barrier to change the magnetization from one easy axis to another is $K = (1/4)K_1 = 1.35 \times 10^5$ erg/cm³. Hence $V_{\text{cr}} = 1.15 \times 10^{-18}$ cm³. We will follow Draine (1996) and take $p = 3$, which was inspired by Billas et al. (1994)'s work showing that small clusters of iron have $3 \mu_B$ per atom. Taking $\rho = 7.87$ g/cm³, we have $N_{\text{cr}} = 9.7 \times 10^4$ and $\hat{\chi}_{\text{max}} = 7.0 \times 10^4$.

4.4. Other forms of iron and summary

Hematite (α -Fe₂O₃) is another possible form of iron, which is more stable than maghemite (γ -Fe₂O₃) discussed above. It is, however, antiferromagnetic, and

perfect crystal can be essentially considered as non-magnetic. In reality, some defects may exist to contribute to the magnetization but it should be negligible comparing with other ferromagnetic materials discussed above. The same goes for FeO. For a summary of magnetic properties of the iron oxides, we refer interested readers to Cornell & Schwertmann (2003), especially their Table 6.2. We do not consider sulfuric iron in this work.

All results discussed above are summarized in Table 1. We can see the maximum cluster size and the enhancement of magnetic susceptibility strongly depends on the form of iron. Even though $\hat{\chi}_{\text{max}}$ on the order of 10^4 is still possible with metallic iron, it is less likely to exist in real dust grains as it can easily be oxidated. We suggest that 10^3 is a more realistic enhancement factor $\hat{\chi}_{\text{max}}$ on the magnetic susceptibility through SPIs.

5. MAGNETIC ALIGNMENT IN PPDS

In Sec. 2, we gave rough estimates of timescales relevant for magnetic alignment and compared them to motivate this study. In this section, we perform a more detailed study on whether magnetic alignment is feasible in a fiducial PPD model.

5.1. Disk model

As an illustration, we adopt the well-known Chiang & Goldreich (1997) model. It is a passive disk with Minimum Mass Solar Nebula density profile $\Sigma = (r/\text{AU})^{-3/2} \Sigma_0$, with $\Sigma_0 = 10^3$ g/cm² (Weidenschilling 1977). It has a superheated surface layer and a cooler interior region, where most grown mm-sized dust grains reside. The temperature in the interior region and the scale height in the model under both hydrostatic equilibrium and radiative equilibrium were fitted as

$$T = \begin{cases} 150 \text{ K} \times \left(\frac{r}{1 \text{ AU}}\right)^{-3/7} & 0.4 \text{ AU} < r < 84 \text{ AU} \\ 21 \text{ K} & 84 < r < 100 \text{ AU} \end{cases}, \quad (17)$$

and

$$\frac{H}{r} = \begin{cases} 0.17 \left(\frac{r}{1 \text{ AU}}\right)^{2/7} & 0.4 \text{ AU} < r < 84 \text{ AU} \\ 0.59 \left(\frac{r}{84 \text{ AU}}\right)^{1/2} & 84 < r < 100 \text{ AU} \end{cases}. \quad (18)$$

At a given radius, the midplane density is used to calculate timescales, which is $\Sigma/\sqrt{2\pi H}$. We adopt a mean molecular weight of 2.3 and assume the temperature to be the same for gas and dust.

For the magnetic field structure, we adopt the estimate from Bai (2011):

$$B = 1.0 \text{ G} \times \left(\frac{\dot{M}}{10^{-8} \text{ M}_{\odot}/\text{yr}}\right)^{1/2} \left(\frac{r}{1 \text{ AU}}\right)^{-11/8}, \quad (19)$$

Material	K (erg/cm ³)	p	V_{cr} (cm ³)	N_{cr}	$\hat{\chi}_{\text{max}}$
Fe ₃ O ₄	6.1×10^5	1.18	2.5×10^{-19}	1.0×10^3	1.1×10^3
γ -Fe ₂ O ₃	1.9×10^5	1.25	8.2×10^{-19}	3.0×10^4	3.7×10^3
Fe	1.35×10^5	3	1.15×10^{-18}	9.7×10^4	7.0×10^4

Table 1. Anisotropy constant K , effective number of Bohr magnetons per iron atom p , critical volume V_{cr} (Eq. (10)), critical cluster size N_{cr} , and reduced magnetic susceptibility $\hat{\chi}_{\text{max}}$ for various iron bearing ferromagnetic materials that may exist in dust grains. See text for discussion and references.

where \dot{M} is the mass accretion rate, which is assumed to be $10^{-8} \text{ M}_{\odot}/\text{yr}$, typical for classical T Tauri stars (see Dutrey et al. 2014 and references therein).

5.2. Timescale comparison

As discussed in Sec. 2.1, we are specially interested in two conditions: $t_L = t_d$, and $t_L = 0.1t_d$. These two conditions define three different regimes:

- $t_L > t_d$: No magnetic alignment.
- $0.1t_d < t_L < t_d$: More complicated dynamical study needed.
- $t_L < 0.1t_d$: Magnetic alignment is possible with fast Larmor precession.

From Eq.(5) and (2):

$$\frac{t_L}{t_d} = 1.65 \times 10^3 \left(\frac{\hat{\chi}}{a_{\text{mm}}} \right)^{-1} \left(\frac{T}{25 \text{ K}} \right)^{3/2} \times \left(\frac{n_g}{5 \times 10^9 \text{ cm}^{-3}} \right) \left(\frac{B}{5 \text{ mG}} \right)^{-1}, \quad (20)$$

where $a_{\text{mm}} \equiv (a/1 \text{ mm})$. We can see that $\hat{\chi}$ and grain size a are degenerate. Due to this degeneracy, the timescale ratio is calculated as a function of radius in the PPD, and the dimensionless factor $\hat{\chi}/a_{\text{mm}}$. The results are plotted in Fig. 2.

First of all, we can see that grains in the inner disk are harder to align compared with those in the outer disk. This is because the gas density power law index (-2.8 in our model within 84 AU) is usually more negative than the magnetic fields power law index (-1.4 in our model). As we decrease the radius, the gaseous damping timescale increases faster than the Larmor precession timescale. In order to achieve fast Larmor precession ($t_L < 0.1t_d$) at a radius of 30 AU, which is the typical resolution of ALMA polarization observations of the nearest star forming regions, we need roughly $\hat{\chi}/a_{\text{mm}} > \sim 10^4$.

This result can be easily translated into more meaningful statements after fixing $\hat{\chi}$. Fig. 3 shows the largest grain sizes with fast Larmor precession ($t_L/t_d < 0.1$) at each radius in the disk. If one take $\hat{\chi} = 10^3$, the upper limit we suggested in Sec. 4, we get $a = 100 \mu\text{m}$. This

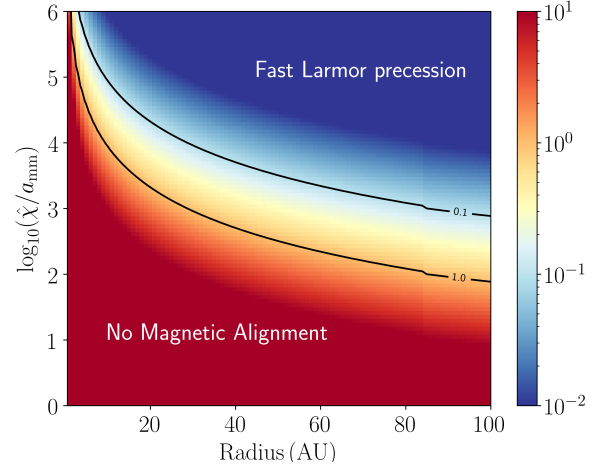


Figure 2. The ratio t_L/t_d as a function of the radius and $\hat{\chi}/a_{\text{mm}}$, with $a_{\text{mm}} \equiv a/(1 \text{ mm})$. The $t_L/t_d = 0.1$ and $t_L/t_d = 1$ contours are plotted to aid the interpretation.

means that grains with sizes of $100 \mu\text{m}$ or bigger are unlikely to be aligned with magnetic field within 30 AU of the central star, even with the aid of SPI. The situation is even worse for regular paramagnetic material ($\hat{\chi} = 1$), where we need $a > 0.1 \mu\text{m}$ to have fast Larmor precession.

The situation is a lot better in the outer disk at scales larger than 100 AU. We will only need $\hat{\chi}/a_{\text{mm}} \sim 10^3$. Alignment of 1 mm dust grains becomes marginally possible if they contain large SPI clusters ($\hat{\chi} > \sim 10^3$).

6. DISCUSSION

6.1. Caveats and uncertainties in this work

The above discussions have relied on a number of simplifying assumptions. In this section we enumerate these assumptions and discuss the implications that relaxing them could have for our results.

6.1.1. Suprathermal rotation

Our first assumption is that the dust grain rotational motions are distributed thermally, meaning that we have effectively ignored the possibility of suprathermal rotation. Purcell (1979) first pointed out that the dust grains can be spun up to suprathermal motion (rotation energy much larger than thermal energy) by torques arising from

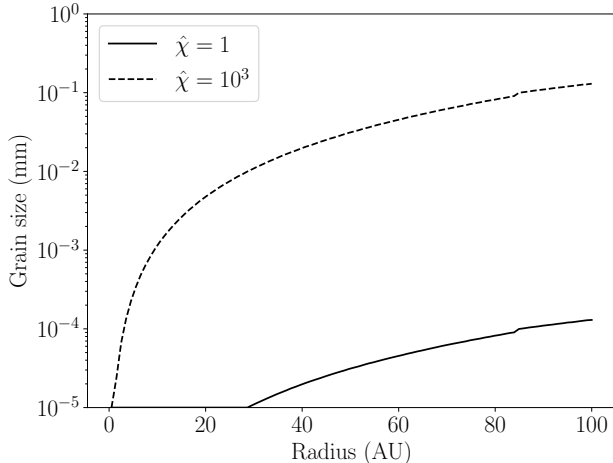


Figure 3. The largest grain sizes with fast Larmor precession ($t_L/t_d < 0.1$) at each radius in the disk. Both regular paramagnetic dust grains ($\hat{\chi} = 1$) and grains with substantial SPIs ($\hat{\chi} = 10^3$) are plotted.

ing from the formation of molecular Hydrogen on the surface of the dust grains. A suprathermally rotating grain would have a larger gaseous damping timescale, which would make grain alignment easier. However, this Hydrogen formation torque is unlikely to work for large millimeter-sized dust grains, since the rotation energy decreases with increasing number of Hydrogen formation sites. In PPDs, more plausible mechanisms for producing suprathermal rotation in millimeter-sized dust grains are radiative alignment torques (RAT; Lazarian & Hoang 2007) and mechanical torques from differential motion with the surrounding gas (MAT; Hoang et al. 2018). Indeed, both Lazarian & Hoang (2007) and Hoang et al. (2018) showed that grains can be aligned towards the so-called “high-J” attractors with angular momenta that are factors of several tens to hundreds of times larger than the thermal angular momentum. However, Hoang et al. (2018) also showed that the mechanical alignment torque goes as $1/\sqrt{N_{\text{facet}}}$, with N_{facet} being the number of facets on the grain surface. This cancellation effect may prevent the MAT from working for large millimeter-sized grains. Such grains may also have limited helicity, which is crucial for both the RAT and the MAT to operate, so it is possible that this cancellation effect applies to RAT as well. More detailed study on suprathermal rotation of large millimeter-sized grains in dense environment is needed to better understand how they might modify our results.

6.1.2. Alignment Condition

Our second assumption is that of fast Larmor precession, coupled with the lack of a precise understand-

ing regarding what constitutes “fast enough” precession. Previous work on magnetic grain alignment has focused on two limiting cases. In the first limit, that of fast Larmor precession ($t_L \ll t_d$), torques are taken to have values that are averaged over the precession cycle prior to investigating grain dynamics (e.g., B-RAT work in Lazarian & Hoang 2007 and B-MAT work in Hoang et al. 2018). In the other limit, that of slow Larmor precession ($t_L \gg t_d$), the effects of magnetic fields are completely ignored (e.g. k-RAT work in Lazarian & Hoang 2007 and k-MAT work in Hoang et al. 2018). However, as we can see from Fig. 2, it is not unreasonable to expect that the ratio t_L/t_d may fall in the range 0.1 – 1 in PPD environments, in which case we can neither assume precession-averaged torques nor ignore the magnetic field completely. Whether dust grains can be aligned magnetically in this regime is thus not currently clear, and this uncertainty limits the predictive power of magnetic alignment theories. Solving this problem will require studying the grain dynamics in three dimensions (i.e., without averaging over Larmor precession) for each potential alignment mechanism.

6.1.3. Form of iron

Our third assumption is the iron abundance. In deriving $\hat{\chi}_{\text{max}}$, we took $f_{sp} = 0.1$. Draine (1996) suggested that about 10% of atoms in a grain are iron atoms. $f_{sp} = 0.1$ means all iron atoms are in the form of SPIs, and no iron atoms are in other forms, such as silicate. This optimistic assumption can easily be wrong and reduce $\hat{\chi}_{\text{max}}$ by one order of magnitude or more, making magnetic alignment harder. We also see that the maximum cluster size depends on the detailed form of iron. Even for ferromagnetic materials, the critical cluster size can vary by orders of magnitude. A chemical study of dust compositions may help resolve this uncertainty.

6.1.4. Disk model

Our fourth assumption is the specific form of the PPD disk model. The MMSN model, by construction, contains only the minimum amount of mass required to form our solar system. It is thus likely to have less mass than a real PPD. Increasing the mass and density of a PPD would increase the gaseous damping timescale, which would make magnetic grain alignment more difficult.

6.2. Effects of temperature dependence on cluster sizes

In Sec. 5, we used $\hat{\chi}$ as a free parameter to discuss the possibility of magnetic alignment in PPDs, even though the $\hat{\chi}_{\text{max}}$ has a temperature dependence. In this section, we discuss the implications of this temperature dependence.

One may be tempted to set $\hat{\chi}$ at each radius in the disk to the local $\hat{\chi}_{\max}$ defined by its local temperature. However, doing so would mean that the SPI sizes in dust grains are changing at each location in the disk, in such a way as to maximize the effects of SPM. This behavior is not physical, both because dust grains at different radii should have similar origins and because the size of SPIs in any given dust grain are unlikely to change as it migrates to other locations of the disk.

However, the temperature dependence of maximum cluster sizes may still have an impact on the magnetic susceptibility of dust grains as a function of disk radius. If the dust grains contain SPIs with sizes larger than the critical N_{cr} (see Eq. 11), then it is possible that these SPIs will be blocked in the low-temperature regions of the disk, while contributing heavily to the magnetic susceptibility in the high-temperature regions of the disk. Such a model would predict a higher degree of magnetic alignment near the center of the disk. It is interesting to note that this behavior is opposite that expected from the usual Curie’s Law (Eq. 3).

In addition to its explicit linear dependence on temperature, the critical volume has another implicit temperature dependence through the anisotropic constant K . For metallic iron, this dependence can be safely ignored as it changes very slowly and smoothly within the temperature range 0–300 K (decreasing by roughly only 15% across the range; Dai & Qian 2017). For magnetite (Fe_3O_4), however, the situation is considerably more complicated. The first complication is that magnetite undergoes a Verwey transition (Verwey 1939; Walz 2002) and thus changes crystal structure at a temperature of around 120 K (Iizumi et al. 1982); the structure changes from cubic spinel above this temperature to monoclinic below it. Our results for magnetite above (Sec. 4) would thus need to be revisited for environments with temperature higher than 120 K. A second complication is that magnetite has so-called “isotropic point” near 130 K. Around this temperature, the cubic anisotropy constant changes signs, such that easy axis changes from the cubic diagonals ($T > 130$ K) to cubic edges ($T < 130$ K); in the immediate vicinity of $T \sim 130$ K, the anisotropy constant is close to zero. A near-zero anisotropy constant permits an arbitrarily large SPI cluster size³. If dust grains contain large clusters of magnetite, they may be blocked at temperatures other than ~ 130 K, in which case our model would

predict a ring of magnetically aligned dust grains only in the region of the disk where $T \approx 130$ K. However, we note that for typical PPDs such a high temperature is reached only on the AU scale (see Eq. 18), which is unlikely to be resolved by ALMA in polarized emission.

6.3. Applications to observed disks

6.3.1. Small grains near the surface of AB Aur disk

Li et al. (2016) used mid-infrared polarimetry to observe the disk around AB Aur at a wavelength of about $10.3\,\mu\text{m}$. The polarization was interpreted as arising from dust grains aligned with poloidal magnetic fields.

At this wavelength, dust grains with sizes on the order of $\sim \mu\text{m}$ are most important for emission. Such small dust grains are lifted more easily by turbulence and thus reach higher above the disk midplane than (sub)millimeter grains. Both the dust grains and the their environment are thus different from what we have discussed in Sec. 5. For the sake of example, suppose the grains are lifted to twice the scale height, where the gas density is an order of magnitude smaller than in the disk midplane. The magnetic field is also likely to be different in this region, but we will assume the same value as in Eq. (19). Given these conditions, we derive the criterion for fast Larmor precession to be $\hat{\chi}/a_{\text{mm}} = 10^3$ at 30 AU (Li et al. 2016 has a 50 AU resolution). For μm -sized grains, SPIs are thus unnecessary to achieve magnetic alignment because $\hat{\chi} = 1$ is sufficient to guarantee fast Larmor precession. Mid-IR polarimetry probing the small dust grains at the disk surface should therefore be capable of studying magnetic field structures in PPD.

6.3.2. Class 0 systems

Class 0 disks represent the earliest stages of planet formation. They are likely to have stronger magnetic fields (Yen et al. 2017) and may be more massive than their later-stage counterparts (Tobin et al. 2020). If we adopt a representative accretion rate, $10^{-6} M_{\odot}/\text{yr}$, we would increase the strength of magnetic field by one order of magnitude, compared with the value adopted in Eq. (19). It is possible that Class 0 disks are also more massive than Class I/II disks. For example, Tobin et al. (2020) reported the mass of Class 0 and Class I disks has mean dust mass of $25.9 M_{\oplus}$ and $14.9 M_{\oplus}$, respectively. If we assume the mass of the Class 0 disk is the same as the one adopted in Sec. 5 – hence the density is also the same – then applying the fast Larmor precession criterion yields $\hat{\chi}/a_{\text{mm}} = 10^3$. Valdivia et al. (2019) infer that the dust grains in Class 0 sources have grown to at least $10\,\mu\text{m}$. Such dust grains require at least $\hat{\chi} = 10$ to have fast Larmor precession, which requires minimal SPI enhancement to achieve. At the same time, $10\,\mu\text{m}$

³ The cluster size may still be limited by the domain size – which is usually larger than the blocking size and which is ignored in this work – as well as other sources of anisotropy such as the shape anisotropy.

dust grains are less efficient at producing polarization through self-scattering at (sub)millimeter wavelengths, avoiding a known confounding effect for studying magnetic fields (Kataoka et al. 2015). Class 0 disks are thus reasonable targets for detecting magnetic fields through spatially resolved (sub)millimeter polarimetry.

7. SUMMARY

In this paper, we discussed the feasibility of magnetic alignment of dust grains with superparamagnetic inclusions in protoplanetary disks. The major results are summarized as follow:

1. Under the Néel’s relaxation theory, we show that there exists a critical size of SPIs within dust grains. SPIs larger than this critical size cannot respond to external magnetic fields and do not contribute to the magnetic susceptibility of the grain. There is thus a maximum enhancement that SPIs can provide to a grain’s magnetic susceptibility, and therefore a corresponding maximum reduction factor for the Larmor precession timescale of the grain.
2. We explore the effect on magnetic susceptibility for a dust grain containing an ensemble of SPIs having a power-law size distribution. We find that if the ensemble contains SPIs bigger than the threshold N_{cr} , the grain as a whole will be unlikely to achieve the maximum magnetic susceptibility χ_{max} (Eq. 13) without fine-tuning (i.e., all SPIs in the dust grain would need to have sizes close to the maximum cluster size). This is because SPIs larger than the critical size do not respond to external magnetic fields and do not contribute to the ensemble magnetic susceptibility (Eq. 12).
3. We estimate the maximum sizes for SPIs composed of several plausible ferromagnetic materials, given their magnetic anisotropy constant at

the temperature of astronomical interest (25 K). Our results are tabulated in Table 1. We suggest that 10^3 is a more realistic upper limit for the SPI enhancement factor $\hat{\chi}$. This value is two orders of magnitude smaller than that obtained from previous work, implying that magnetic alignment is more difficult than previously thought.

4. We explore the feasibility of magnetic grain alignment in the disk midplane of a MMSN model for a PPD. We find that (1) magnetic alignment is impossible unless SPIs are ubiquitous throughout the disk, even if the dust grains are as small as $10 \mu\text{m}$; (2) it is difficult to align grains larger than $100 \mu\text{m}$ even with SPIs, particularly at small orbital radii where the high gas density leads to short damping timescales.

We conclude that large millimeter-sized dust grains in the midplane of PPDs are unlikely to be aligned with the ambient magnetic fields (c.f. Fig. 3). An important implication of this finding is that observations that are primarily sensitive to the emission from this population of grains – such as (sub)millimeter-wavelength polarimetric observations of Class I/II PPDs – are unlikely to be tracing the disk magnetic field structure. We suggest instead that observations of disk surfaces – probed by mid-infrared polarimetry – and the early Class 0 PPDs are better-suited to studying the magnetic fields structures in PPDs.

ACKNOWLEDGEMENTS

We thank the anonymous referee for detailed and constructive comments that greatly improved the manuscript. We thank Xuening Bai, Zhi-Yun Li, Daniel Harsono, and Vincent Guillet for fruitful discussions. We thank Zheng Liu, Zhiyuan Yao and Shuai Yin for discussions over the physics behind the superparamagnetism. We thank Dominic Pesce, Zhi-Yun Li, and Xuening Bai for comments and suggestions that helped to improve the manuscript.

APPENDIX

A. A SIMPLE MODEL FOR SPI DYNAMICS

In order to see how the magnetic susceptibility of an ensemble of identical SPIs changes as a function of their volume, we use a simplified model with three-axis assumption: all the SPIs have their easy axis along one of an arbitrary set of Cartesian axes and they are split evenly among three axes. Also, we are interested in the regime where $V > kT/K$, so the equilibrium state have averaged magnetic moment as $\mu^2 B/kT$ along easy axis and 0 along perpendicular directions. Initially, all the SPIs have their magnetic moment randomly distributed, so that there are equal numbers of μ ’s along the six directions ($\pm x$, $\pm y$, and $\pm z$).

Now let’s apply magnetic field B along z axis at $t = 0$. Since the Barnett equivalent field (for thermal angular velocity of a $10 \mu\text{m}$ dust grain) $H_B = \Omega/\gamma \sim 10^{-7}$ Oersted and the corresponding magnetic energy is at most on

the order of $10^5 \mu_B H_B / k \sim 10^{-7}$ K, which is very small compared with the thermal energy (on the order of 10 K). We conclude that the magnetic field cannot overcome the anisotropy energy on its own, which is even bigger than the thermal energy. We need the Brownian-like process Néel proposed that each magnetic moment tries to change its orientation every t_0 . Since the SPIs with easy axis along x or y direction cannot response to the magnetic field along z direction, we focus on those with easy axis along z axis, and define f_+ and f_- as fraction of particles along $z+$ and $z-$, respectively. The energies for these two states are $-\mu B$ and μB , but there is an energy barrier of KV if the magnetic moment tries to switch to the opposite state. As such, the probability of one successful transition is:

$$\begin{cases} P(z+ \rightarrow z-) = \exp\left(-\frac{KV + \mu B}{kT}\right) \\ P(z- \rightarrow z+) = \exp\left(-\frac{KV - \mu B}{kT}\right) \end{cases}. \quad (\text{A1})$$

The dynamical equation for (f_+, f_-) is then:

$$\frac{d}{dt} \begin{pmatrix} f_+ \\ f_- \end{pmatrix} = \frac{1}{t_0} \begin{pmatrix} -\exp\left(-\frac{KV + \mu B}{kT}\right) & \exp\left(-\frac{KV - \mu B}{kT}\right) \\ \exp\left(-\frac{KV + \mu B}{kT}\right) & -\exp\left(-\frac{KV - \mu B}{kT}\right) \end{pmatrix} \begin{pmatrix} f_+ \\ f_- \end{pmatrix}. \quad (\text{A2})$$

The solution to this equation is:

$$\begin{pmatrix} f_+ \\ f_- \end{pmatrix} = \exp\left(\frac{t}{t_N} \mathcal{M}\right) \begin{pmatrix} f_{+,0} \\ f_{-,0} \end{pmatrix}, \quad (\text{A3})$$

where t_N is the Néel's relaxation timescale, and \mathcal{M} is a matrix defined as $\mathcal{M} \equiv [[-e^{-\beta}, e^{\beta}], [e^{-\beta}, -e^{\beta}]]$, with $\beta \equiv \mu B / kT$.

It is possible to calculate the above matrix exponential explicitly with the aid of the following matrix transformation:

$$\mathcal{M} = \mathcal{P} \begin{pmatrix} 0 & 0 \\ 0 & -2 \cosh \beta \end{pmatrix} \mathcal{P}^{-1}, \quad (\text{A4})$$

with $\mathcal{P} \equiv [[e^{\beta}, 1], [e^{-\beta}, -1]]$. Eq. (A3) can then be rewritten as:

$$\begin{pmatrix} f_+ \\ f_- \end{pmatrix} = \mathcal{P} \begin{pmatrix} 1 & 0 \\ 0 & \exp\left(-\frac{2t}{t_N} \cosh \beta\right) \end{pmatrix} \mathcal{P}^{-1} \begin{pmatrix} f_{+,0} \\ f_{-,0} \end{pmatrix}. \quad (\text{A5})$$

Now let's consider the two limiting cases. For $t \gg t_N$, the exponential in Eq. (A5) is basically 0. We have:

$$\begin{pmatrix} f_+ \\ f_- \end{pmatrix} = \frac{f_{+,0} + f_{-,0}}{2 \cosh \beta} \begin{pmatrix} e^{\beta} \\ e^{-\beta} \end{pmatrix}. \quad (\text{A6})$$

This means the end state is independent of initial state and the system has reached equilibrium (we always have $f_{+,0} + f_{-,0} = 1$). In this case, the averaged magnetic moment along magnetic field direction is $\langle \mu_z \rangle = f_+ \mu - f_- \mu = \mu \tanh \beta \approx \mu^2 B / kT$. The magnetic susceptibility of this ensemble is thus the same as the superparamagnetic magnetic susceptibility χ_{sp} in Eq. (7) (remember that there are two third of SPIs with perpendicular easy axes and do not contribute to the magnetic susceptibility).

For $t \ll t_N$, we have (this is easier to derive directly from Eq. A3):

$$\begin{pmatrix} f_+ \\ f_- \end{pmatrix} \approx \left(\mathcal{I} + \frac{t}{t_N} \mathcal{M}\right) \begin{pmatrix} f_{+,0} \\ f_{-,0} \end{pmatrix} = \begin{pmatrix} f_{+,0} \\ f_{-,0} \end{pmatrix} + \frac{t}{t_N} \begin{pmatrix} -f_{+,0} e^{-\beta} + f_{-,0} e^{\beta} \\ f_{+,0} e^{-\beta} - f_{-,0} e^{\beta} \end{pmatrix}. \quad (\text{A7})$$

From the end result, we can see that a fraction of $(t/t_N)e^{-\beta}$ SPIs have changed from $+$ state to $-$ state, whereas a fraction of $(t/t_N)e^{\beta}$ SPIs have changed from $-$ state to $+$ state. In this case, for an initial condition $f_{+,0} = f_{-,0} = 0.5$, we get $\langle \mu_z \rangle = f_+ \mu - f_- \mu = (2t\mu/t_N) \sinh \beta \approx (2t/t_N) \mu^2 B / kT$.

The accurate solution, together with the above two asymptotic solutions, is plotted in Fig. 4. μ_z linearly increases to its equilibrium value. However, since the Néel's relaxation timescale increases exponentially with the volume V , the

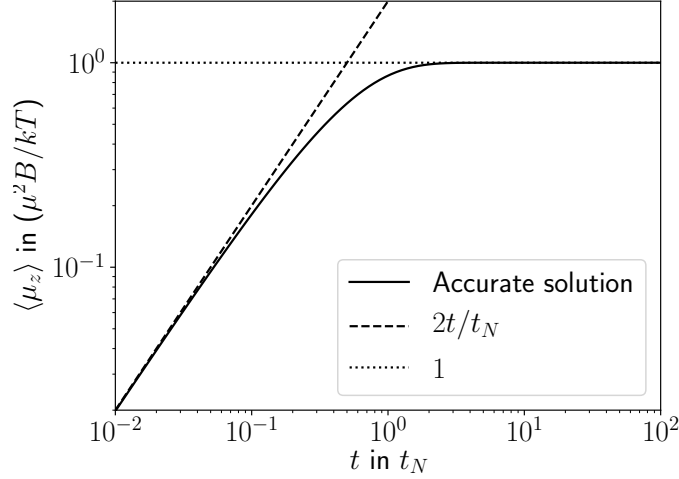


Figure 4. The averaged magnetic moment along magnetic field direction $\langle \mu_z \rangle$ of SPIs with magnetic moment μ and Néel's relaxation timescale t_N , as a function of time t exposed in an external magnetic field B . The SPIs considered here all have their easy axis along the magnetic field direction $\pm z$.

magnetic susceptibility of the ensemble of SPIs changes with volume V very sharply across the critical volume defined in Eq. (10) which, to a good approximation, can be summarized as follows:

$$\chi = \begin{cases} 0, & V > V_{\text{cr}} \\ \chi_{sp}, & V < V_{\text{cr}} \end{cases}. \quad (\text{A8})$$

REFERENCES

- Abe, K., Miyamoto, Y., & Chikazumi, S. 1976, *Journal of the Physical Society of Japan*, 41, 1894, doi: [10.1143/JPSJ.41.1894](https://doi.org/10.1143/JPSJ.41.1894)
- Alves, F. O., Girart, J. M., Padovani, M., et al. 2018, *A&A*, 616, A56, doi: [10.1051/0004-6361/201832935](https://doi.org/10.1051/0004-6361/201832935)
- Andersson, B. G., Lazarian, A., & Vaillancourt, J. E. 2015, *ARA&A*, 53, 501, doi: [10.1146/annurev-astro-082214-122414](https://doi.org/10.1146/annurev-astro-082214-122414)
- Bacciotti, F., Girart, J. M., Padovani, M., et al. 2018, *ApJL*, 865, L12, doi: [10.3847/2041-8213/aadf87](https://doi.org/10.3847/2041-8213/aadf87)
- Bai, X.-N. 2011, *ApJ*, 739, 50, doi: [10.1088/0004-637X/739/1/50](https://doi.org/10.1088/0004-637X/739/1/50)
- Barnett, S. J. 1915, *Physical Review*, 6, 239, doi: [10.1103/PhysRev.6.239](https://doi.org/10.1103/PhysRev.6.239)
- Bean, C. P., & Livingston, J. D. 1959, *Journal of Applied Physics*, 30, S120, doi: [10.1063/1.2185850](https://doi.org/10.1063/1.2185850)
- Billas, I. M., Châtelain, A., & de Heer, W. A. 1994, *Science*, 265, 1682, doi: [10.1126/science.265.5179.1682](https://doi.org/10.1126/science.265.5179.1682)
- Chiang, E. I., & Goldreich, P. 1997, *ApJ*, 490, 368, doi: [10.1086/304869](https://doi.org/10.1086/304869)
- Coey, J. M. D., & Khalafalla, D. 1972, *Phys. Stat. Sol. (a)*, 11, 229
- Cornell, R. M., & Schwertmann, U. 2003, *The Iron Oxides: Structure, Properties, Reactions, Occurrences and Uses* (Wiley-VCH Verlag GmbH & Co. KGaA)
- Cox, E. G., Harris, R. J., Looney, L. W., et al. 2018, *ApJ*, 855, 92, doi: [10.3847/1538-4357/aaacd2](https://doi.org/10.3847/1538-4357/aaacd2)
- Dai, D., & Qian, K. 2017, *Ferromagnetism* (in Chinese) (Beijing: Science Press)
- Davis, Jr., L., & Greenstein, J. L. 1951, *ApJ*, 114, 206, doi: [10.1086/145464](https://doi.org/10.1086/145464)
- Dent, W. R. F., Pinte, C., Cortes, P. C., et al. 2019, *MNRAS*, 482, L29, doi: [10.1093/mnrasl/sly181](https://doi.org/10.1093/mnrasl/sly181)
- Dolginov, A. Z., & Mytrophanov, I. G. 1976, *Ap&SS*, 43, 257, doi: [10.1007/BF00640009](https://doi.org/10.1007/BF00640009)
- Draine, B. T. 1996, *Astronomical Society of the Pacific Conference Series*, Vol. 97, *Optical and Magnetic Properties of Dust Grains*, ed. W. G. Roberge & D. C. B. Whittet, 16
- Draine, B. T. 2004, *Astrophysics of Dust in Cold Clouds*, ed. D. Pfenniger & Y. Revaz (Berlin, Heidelberg: Springer Berlin Heidelberg), 213–304. https://doi.org/10.1007/3-540-31636-1_3
- Draine, B. T., & Hensley, B. 2013, *ApJ*, 765, 159, doi: [10.1088/0004-637X/765/2/159](https://doi.org/10.1088/0004-637X/765/2/159)

- Draine, B. T., & Weingartner, J. C. 1997, *ApJ*, 480, 633, doi: [10.1086/304008](https://doi.org/10.1086/304008)
- Dutrey, A., Semenov, D., Chapillon, E., et al. 2014, in *Protostars and Planets VI*, ed. H. Beuther, R. S. Klessen, C. P. Dullemond, & T. Henning, 317
- Goodman, A. A., & Whittet, D. C. B. 1995, *ApJL*, 455, L181, doi: [10.1086/309840](https://doi.org/10.1086/309840)
- Hiltner, W. A. 1949, *Nature*, 163, 283, doi: [10.1038/163283a0](https://doi.org/10.1038/163283a0)
- Hoang, T. 2017, arXiv e-prints, arXiv:1704.01721. <https://arxiv.org/abs/1704.01721>
- Hoang, T., Cho, J., & Lazarian, A. 2018, *ApJ*, 852, 129, doi: [10.3847/1538-4357/aa9edc](https://doi.org/10.3847/1538-4357/aa9edc)
- Hull, C. L. H., & Zhang, Q. 2019, *Frontiers in Astronomy and Space Sciences*, 6, 3, doi: [10.3389/fspas.2019.00003](https://doi.org/10.3389/fspas.2019.00003)
- Hull, C. L. H., Yang, H., Li, Z.-Y., et al. 2018, *ApJ*, 860, 82, doi: [10.3847/1538-4357/aabfeb](https://doi.org/10.3847/1538-4357/aabfeb)
- Iizumi, M., Koetzle, T. F., Shirane, G., et al. 1982, *Acta Cryst.*, B38, 2121
- Jones, R. V., & Spitzer, Lyman, J. 1967, *ApJ*, 147, 943, doi: [10.1086/149086](https://doi.org/10.1086/149086)
- Kataoka, A., Tsukagoshi, T., Pohl, A., et al. 2017, *ApJL*, 844, L5, doi: [10.3847/2041-8213/aa7e33](https://doi.org/10.3847/2041-8213/aa7e33)
- Kataoka, A., Muto, T., Momose, M., et al. 2015, *ApJ*, 809, 78
- Kataoka, A., Tsukagoshi, T., Momose, M., et al. 2016, *ApJ*, 831, L12
- Lazarian, A. 2007, *JQSRT*, 106, 225, doi: [10.1016/j.jqsrt.2007.01.038](https://doi.org/10.1016/j.jqsrt.2007.01.038)
- Lazarian, A., & Hoang, T. 2007, *MNRAS*, 378, 910, doi: [10.1111/j.1365-2966.2007.11817.x](https://doi.org/10.1111/j.1365-2966.2007.11817.x)
- Li, D., Pantin, E., Telesco, C. M., et al. 2016, *ApJ*, 832, 18, doi: [10.3847/0004-637X/832/1/18](https://doi.org/10.3847/0004-637X/832/1/18)
- Li, Y., Montano, P., Barbiellini, B., et al. 2007, *Journal of Physics and Chemistry of Solids*, 68, 1556, doi: <https://doi.org/10.1016/j.jpcs.2007.03.037>
- Lin, Z.-Y. D., Li, Z.-Y., Yang, H., et al. 2019, arXiv e-prints, arXiv:1912.10012. <https://arxiv.org/abs/1912.10012>
- Mathewson, D. S., & Ford, V. L. 1970, *MmRAS*, 74, 139
- Mathis, J. S. 1986, *ApJ*, 308, 281, doi: [10.1086/164499](https://doi.org/10.1086/164499)
- Morrish, A. H. 2001, *The Physical Principles of Magnetism* (Wiley-IEEE Press)
- Néel, L. 1949, *Ann. Géophys.*, 5, 99
- Ohashi, S., & Kataoka, A. 2019, *ApJ*, 886, 103, doi: [10.3847/1538-4357/ab5107](https://doi.org/10.3847/1538-4357/ab5107)
- Ohashi, S., Kataoka, A., Nagai, H., et al. 2018, *ApJ*, 864, 81, doi: [10.3847/1538-4357/aad632](https://doi.org/10.3847/1538-4357/aad632)
- Pisane, K. L., Singh, S., & Seehra, M. S. 2017, *Applied Physics Letters*, 110, 222409, doi: [10.1063/1.4984903](https://doi.org/10.1063/1.4984903)
- Planck Collaboration, Ade, P. A. R., Aghanim, N., et al. 2015, *A&A*, 576, A104, doi: [10.1051/0004-6361/201424082](https://doi.org/10.1051/0004-6361/201424082)
- Purcell, E. M. 1979, *ApJ*, 231, 404, doi: [10.1086/157204](https://doi.org/10.1086/157204)
- Roberge, W. G., Degraff, T. A., & Flaherty, J. E. 1993, *ApJ*, 418, 287, doi: [10.1086/173390](https://doi.org/10.1086/173390)
- Stephens, I. W., Looney, L. W., Kwon, W., et al. 2014, *Nature*, 514, 597
- Stephens, I. W., Yang, H., Li, Z.-Y., et al. 2017, *ApJ*, 851, 55, doi: [10.3847/1538-4357/aa998b](https://doi.org/10.3847/1538-4357/aa998b)
- Tazaki, R., Lazarian, A., & Nomura, H. 2017, *ApJ*, 839, 56, doi: [10.3847/1538-4357/839/1/56](https://doi.org/10.3847/1538-4357/839/1/56)
- Tobin, J. J., Sheehan, P. D., Megeath, S. T., et al. 2020, *ApJ*, 890, 130, doi: [10.3847/1538-4357/ab6f64](https://doi.org/10.3847/1538-4357/ab6f64)
- Valdivia, V., Maury, A., Brauer, R., et al. 2019, *MNRAS*, 488, 4897, doi: [10.1093/mnras/stz2056](https://doi.org/10.1093/mnras/stz2056)
- Verwey, E. J. W. 1939, *Nature*, 144, 327
- Walz, F. 2002, *Journal of Physics: Condensed Matter*, 14, R285, doi: [10.1088/0953-8984/14/12/203](https://doi.org/10.1088/0953-8984/14/12/203)
- Weidenschilling, S. J. 1977, *Ap&SS*, 51, 153, doi: [10.1007/BF00642464](https://doi.org/10.1007/BF00642464)
- Yang, H., Li, Z.-Y., Looney, L., & Stephens, I. 2016a, *MNRAS*, 456, 2794
- Yen, H.-W., Koch, P. M., Takakuwa, S., et al. 2017, *The Astrophysical Journal*, 834, 178, doi: [10.3847/1538-4357/834/2/178](https://doi.org/10.3847/1538-4357/834/2/178)